VU VRIJE UNIVERSITEIT AMSTERDAM

VU Research Portal

Quantitative PET/CT imaging and dosimetry of 89Zr labelled compounds

Makris, N.

2015

document version
Publisher's PDF, also known as Version of record

Link to publication in VU Research Portal

citation for published version (APA)
Makris, N. (2015). *Quantitative PET/CT imaging and dosimetry of 89Zr labelled compounds*. [PhD-Thesis - Research and graduation internal, Vrije Universiteit Amsterdam].

General rights
Copyright and moral rights for the publications made accessible in the public portal are retained by the authors and/or other copyright owners and it is a condition of accessing publications that users recognise and abide by the legal requirements associated with these rights.

- Users may download and print one copy of any publication from the public portal for the purpose of private study or research.
- You may not further distribute the material or use it for any profit-making activity or commercial gain
- You may freely distribute the URL identifying the publication in the public portal ?

Take down policy
If you believe that this document breaches copyright please contact us providing details, and we will remove access to the work immediately and investigate your claim.

E-mail address:
vuresearchportal.ub@vu.nl

Download date: 05. May. 2023

4

PET/CT derived whole body and bone marrow dosimetry of ^{89}Zr-cetuximab

Nikolaos E. Makris, Ronald Boellaard, Arthur van Lingen,
Adriaan A. Lammertsma, Guus A.M.S. van Dongen, Henk M. Verheul,
Catharina W. Menke and Marc C. Huisman

This study was originally published in Journal of Nuclear Medicine. *Nikolaos E. Makris, Ronald Boellaard, Arthur van Lingen, Adriaan A. Lammertsma, Guus A.M.S. van Dongen, Henk M. Verheul, Catharina W. Menke and Marc C. Huisman. PET/CT derived whole body and bone marrow dosimetry of ^{89}Zr-cetuximab. J Nucl Med (2015) 56:249-254*

Abstract

PET/CT imaging allows for image based estimates of organ and red marrow (RM) residence times. The aim of this study was to derive PET/CT based radiation dosimetry for ^{89}Zr-cetuximab, with special emphasis on determining RM absorbed dose.

Methods: Seven patients with colorectal cancer received 36.9 ± 0.8 MBq ^{89}Zr-cetuximab within 2 h after administration of a therapeutic dose of 500 mg·m^{-2} of cetuximab. Whole body PET/CT scans and blood samples were obtained at 1, 24, 48, 94, and 144 h after injection. RM activity concentrations were calculated from manual delineation of the lumbar vertebrae and blood samples, assuming a fixed RM to plasma activity concentration ratio (RMPR) of 0.19

The cumulated activity was calculated as the area under the curve of the organ time-activity data (liver, lungs, kidneys, spleen, and RM), assuming physical decay after the last scan. The residence time for each organ was derived by dividing the cumulated activity with the total injected activity. The residence time in the remainder of the body was calculated as the maximum possible residence time minus the sum of residence time of source organs, assuming no excretion during the time course of the scans. The (self and total) RM and organ absorbed doses and effective whole body radiation dose were obtained using dose conversion factors from OLINDA/EXM 1.1. Several simplified 3 time-point dosimetry approaches were also evaluated.

Results: The first approach yielded self and total RM doses of 0.17 ± 0.04 and 0.51 ± 0.06 mGy·MBq^{-1}, respectively. The second approach deviated by –21% in self dose and –6% in total dose. RMPR increased over time in 5 out of 7 patients. The highest ^{89}Zr absorbed dose was observed in liver with 2.60 ± 0.78 mGy·MBq^{-1}, followed by the kidneys, spleen, and lungs, whereas the effective whole body dose was 0.61 ± 0.09 mSv·MBq^{-1}. The simplified 3 time-point (1, 48, and 144 h) dosimetry approach deviated by at most 4% in both organ absorbed doses and effective dose.

Conclusions: Although the total RM dose estimates obtained with the 2 approaches differed only by at most 6%, the image based approach is preferred because it accounts for nonconstant RMPR. The number of successive scans can be reduced to 3 without affecting effective dose estimates.

4.1 Introduction

Positron Emission Tomography (PET) using long lived radionuclides has proven to be a valuable tool for predicting the biodistribution of labelled monoclonal antibodies (mAb) (1,2) and organ dosimetry for radioimmunotherapy (2). In addition, the dose limiting tissue can be determined, enabling dose escalation and optimization of therapeutic treatment planning. In particular, a recent study showed that the biodistributions of ^{89}Zr-Df-cetuximab and ^{88}Y-DOTA-cetuximab (^{88}Y as a substitute for ^{90}Y) were comparable for all organs (1). Another study from the same group demonstrated nearly identical biodistributions of ^{89}Zr-ibritumomab and ^{90}Y-ibritumomab (2). Recently, the effect of radio-immunotherapy using ^{90}Y-cetuximab (combined with external-beam irradiation) on local tumour control *in vivo* was examined in 3 human squamous cell carcinoma models (3). The latter study showed that PET imaging using ^{86}Y-cetuximab may be used to assess EGFR expression, which in turn could be a potential predictor for response to combined radio-immunotherapy and external beam radiotherapy. With radioimmunotherapy, bone marrow can be the dose-limiting organ. Conventionally, the red marrow (RM) activity concentration is assumed to be 19% of the plasma activity concentration (4). Assuming a hematocrit value of 0.44, the RM to blood ratio (RMBLR) will be assigned a value of 0.34. However, recent studies by Schwartz et al. (5) and Hindorf et al. (6) have reported a time dependent RM to plasma activity concentration ratio (RMPR) based on PET imaging using ^{124}I-cG250 and ^{124}I-huA33 and scintigraphic imaging using ^{131}I-labelled anti-CD22 mAb, respectively. This increase in RMPR may reflect binding to Fc receptor-expressing cells in bone marrow. Those observations imply that RM dose estimates based on blood or plasma activity concentrations may be inappropriate, at least for some mAbs. Schwartz et al. (5) reported that the plasma based approach can produce discrepancies of as much as –74 to +62% in individual patients for self RM dose (after ^{124}I-labelled mAb administration), as compared with PET/CT image based dosimetry. It has also been reported that ^{124}I-labelled mAbs tend to release free radionuclides on antibody internalization, resulting in rapid clearance of the radionuclides from the target tissue, leading to reduced tumour contrast (7) and a change in RMPR over time. Unlike ^{124}I, ^{89}Zr appears to be a residualizing radiometal potentially circumventing these problems (7). However, increased radioactivity in bone, as reported in recent studies (8,9) using ^{89}Zr as a PET tracer, has not been analysed adequately yet to assess whether or not *in vivo* metal release or other mechanisms are involved. Again, a consequence could be that the assumption of a constant RMPR is

wrong.

The novelty of this study lies in the exploration of the added potential of performing a PET/CT derived biodistribution/dosimetry in humans for a mAb labelled with a positron emitter. The advantage of the associated (low-dose) computed tomography (CT) scan is more robust organ delineation. In addition, use of a CT defined volume of interest (VOI) of the lumbar vertebrae may allow for noninvasive quantification of RM activity concentrations. The aim of this study was to assess biodistribution and radiation dosimetry of ^{89}Zr-cetuximab in humans, with a special emphasis on a comparison of image and plasma based RM dose estimation approaches.

4.2 Materials and methods

4.2.1 Imaging protocol

Seven patients (4 men, 3 women) with histopathologically confirmed advanced kRas wild-type colorectal cancer (Table 4.1) received 36.9 ± 0.8 MBq of ^{89}Zr-cetuximab within 2 h after administration of the first therapeutic dose of 500 mg·m^{-2} of cetuximab. PET/CT scans (Gemini TF-64; Philips Healthcare) and blood samples were obtained at 1, 24, 48, 94, and 144 h after injection (10). PET data were normalized; corrected for decay, randoms, dead time, scatter and attenuation; and reconstructed using a time-of-flight list-mode ordered-subsets expectation maximization reconstruction method with a matrix size of 144 × 144 and a voxel size of 4 × 4 × 4 mm^3. In addition, for each time point, a 50 mAs low dose CT scan was acquired for attenuation correction purposes. Corresponding CT images were reconstructed with an image matrix size of 512 × 512 and a voxel size of 1.17 × 1.17 × 5 mm^3. For the present analysis, all 5 CT scans for each patient were

Table 4.1. *Patient details*

Sex	Weight(kg)	Residence time in blood(h)	Whole body to blood cumulated activity ratio
M	72	44	2.1
M	82	47	2.1
M	79	35	2.5
M	79	26	3.4
F	75	43	2.2
F	93	40	2.5
F	69	56	1.8

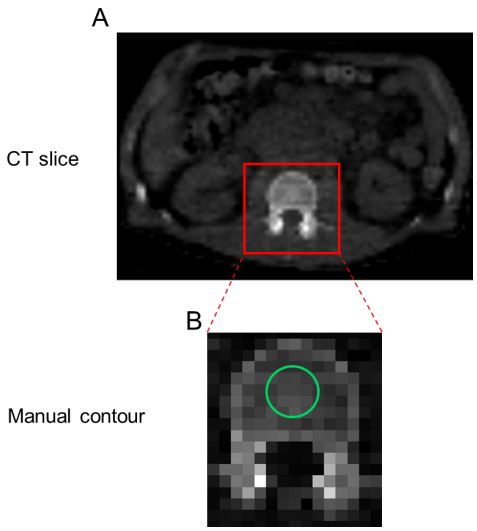

Figure 4.1. *Original CT slice (A) and axial CT slice (B) with manually defined LV contour (green line) enclosing the intraosseous volume*

re-binned into a 4 × 4 × 4 mm^3 voxel size to map CT VOIs onto the PET images. The study was approved by the Medical Ethics Committee of the VU University Medical Centre, and all patients signed a written informed consent form before the inclusion.

4.2.2 Organ dosimetry

The activity for each organ that was visible in all PET scans (liver, lungs, kidneys, spleen, and RM) was determined using the mean activity concentration in VOIs using in-house developed software. VOIs were independently drawn on all 5 CT scans for each patient and subsequently mapped onto the respective PET scans. Total organ activities were derived using standard organ masses as reported by Stabin et al. (11). The cumulated activity was calculated as the area under the curve of the organ time-activity data approximated by the trapezoidal rule and assuming only physical decay after the last measurement. Next, the residence time was derived by dividing the cumulated activity by the total injected activity. The residence time in the remainder of the body was calculated as the maximum residence time (based on physical decay only) minus the sum of residence time of source organs (an organ was designated as source organ when uptake was visible), assuming no excretion during the time course of the scans. Although the effective total residence time could also be derived from a whole body VOI (on average 35% lower values), this approach was not followed to obtain conservative estimates of the effective dose. Individual residence times were scaled with

Table 4.2. *Parameters overview*

Parameters	Definition
$\tilde{A}_{RM}$	Cumulated activity concentration in the RM
$\tilde{A}_{PL}$	Cumulated activity concentration in the plasma
$\tilde{A}_{RM}$	Cumulated activity in the RM
$\tilde{A}_{WB}$	Cumulated activity in the whole body
$\tilde{A}_{RB}$	Cumulated activity in the remainder of the body
RMPR	RM to plasma activity concentration ratio
RMECFF	RM to extracellular fluid activity concentration fraction
$m_{RM-patient}$	Patient specific RM mass
$m_{WB-patient}$	Patient specific whole body mass
$m_{RM-MIRDOSE3}$	Standard RM mass
$m_{WB-MIRDOSE3}$	Standard whole body mass
$D_{RM}{}^{Self}$	Self RM dose
$D_{RM}{}^{Cross}$	Cross RM dose
$D_{RM}{}^{Total}$	Total RM dose
S(RM ← RM)	Dose conversion factor for RM to RM contribution
S(RM ← RB)	Dose conversion factor for remainder body to RM contribution
S(RM ← WB)	Dose conversion factor for whole body to RM contribution
HU	Hounsfield unit

the mass ratio of the patient to reference man/woman before being used as input in OLINDA/EXM 1.1. This software was used for calculation of organ absorbed doses and effective dose (11).To derive a simplified dosimetry protocol with 3 time points, all possible combinations were tested for the ability to estimate organs absorbed doses and effective doses as accurate as possible.

4.2.3 RM dose estimation methods

Blood-based method

Conventionally, the blood based approach assumes that plasma activity concentration is equal to the extracellular fluid activity concentration in the marrow space and, therefore, that RMPR is constant, equal to the fraction of RM composed of extracellular fluid (RMECFF) (4). In this method, a fixed, time-independent RMPR value of 0.19 is used. In Table 4.2, a parameter overview can be found. Plasma samples were counted in a Wallac 1470 well counter (Perkin Elmer Lifescience) and conversion of the derived counts per minute to disintegration per minute was done (a description of the methodology of cross calibration between the PET scanner and the well counter can be found in Greuter et al. (12)). The total cumulated activity concentration in the RM is given by:

$$\left[\tilde{A}_{RM}\right] = RMECFF \times \left[\tilde{A}_{PL}\right] \tag{4.1}$$

or alternatively the cumulated activity can be written as:

$$\tilde{A}_{RM} = RMECFF \times \left[\tilde{A}_{PL}\right] \times m_{RM-patient} \tag{4.2}$$

The RM mass can be approximated through the standard adult and patient specific whole body mass:

$$m_{RM-patient} = \frac{m_{RM-MIRDOSE3}}{m_{WB-MIRDOSE3}} \times m_{WB-patient} \tag{4.3}$$

$$\tilde{A}_{RM} = RMECFF \times \left[\tilde{A}_{PL}\right] \times \frac{m_{RM-MIRDOSE3}}{m_{WB-MIRDOSE3}} \times m_{WB-patient} \tag{4.4}$$

where $m_{RM-MIRDOSE3}$, $m_{WB-MIRDOSE3}$ and $m_{WB-patient}$ correspond to the standard adult mass for RM (men: 1.12 kg, women: 1.30 kg), whole body (m: 73.7 kg, f: 58.0 kg) (11), and the patient specific whole body mass, respectively (See Table 4.2). The total RM absorbed dose can be divided into 2 contributions, the self RM dose–which represents the dose from the marrow spaces–and the cross RM dose–which represents the dose from the remaining tissues of the body (13, 14). This can be expressed by the following equations:

$$D_{RM}^{Total} = D_{RM}^{Self} + D_{RM}^{Cross} \tag{4.5}$$

$$D_{RM}^{Total} = \tilde{A}_{RM} \times S\left(RM \leftarrow RM\right) + \left(\tilde{A}_{WB} - \tilde{A}_{RM}\right) \times S\left(RM \leftarrow RB\right) \tag{4.6}$$

The full expressions of self dose and cross dose contribution to the RM can be obtained by substituting Equations 4.2, 4.3 and 4.4 into 4.6. By introducing a mass scaling for the S factors in Equation 4.6, the $m_{WB-patient}$ terms cancel out and a patient mass independent term remains, whereas the final cross RM dose term will be patient mass dependent. Calculations and full expression of the formulas can be found in the Appendix.

Manual VOI delineation method

In immunoPET studies, a second approach to determine $[\tilde{A}_{RM}]$ is by delineating VOIs in each of the 5 (L1-L5) segments of the lumbar vertebrae (LV) on CT slices (Figure 4.1). Each VOI had a spheric shape with a volume of

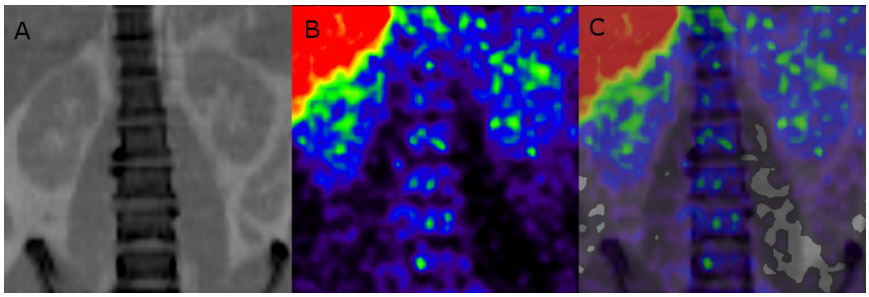

Figure 4.2. *Typical example of coronal slices of CT (A), PET (B), and PET/CT (C).*

6 mL, providing a total volume of 30 mL for all 5 segments. Subsequently, all 5 VOIs were transferred to the PET images, and the mean activity concentration was calculated. The effect of using smaller or larger volumes in estimating mean activity concentration was also investigated. The LV consists of compact bone, trabecular bone, and marrow space elements–that is, red and yellow marrow, extracellular fluid, and vasculature. Assuming that there is no specific binding of the radiolabelled antibody cetuximab to trabecular bone, it follows that the trabecular bone activity concentration should be zero. Thus, a correction factor was applied for the presence of trabecular bone in the LV segments. To this end, the RM activity concentration was scaled based on the volume of the LV composed of trabecular bone (f_{tb};men, 0.135; women, 0.148) (15), thus a multiplicative correction factor 1/1-f_{tb} was applied. This approach does not assume a constant RMPR over time as it is an image derived method. Equation 4.4 was adjusted by replacing RMECFF×$[\tilde{A}_{PL}]$ with $[\tilde{A}_{RM}]$, as the RM activity concentration

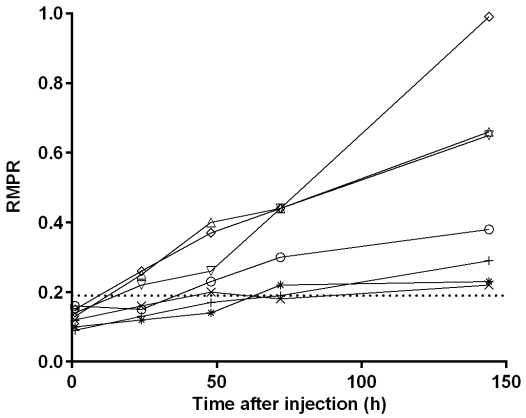

Figure 4.3. *Image derived RMPR as function of imaging time after injection of ^{89}Zr-cetuximab. Five out of 7 patients depict increasing RMPR as function of time, and only in 2 patients RMPR corresponds with the nominal value of 0.19 (dotted line).*

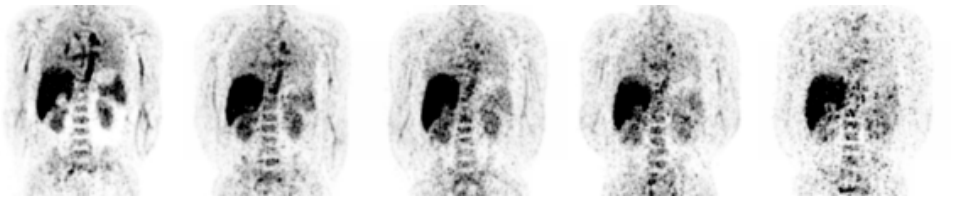

Figure 4.4. *Biodistribution of ^{89}Zr-cetuximab as visualized using PET during the course of 7 d (left to right: 1, 24, 48, 72, 144 h after injection). Data are decay corrected to the time of injection.*

was directly obtained from the PET images. Visual inspection of the PET images did not show higher uptake in the compact bone component when compared with the marrow space elements of the LV (Figure 4.2).

4.3 Results

Figure 4.3 shows RMPR as a function of time for patients injected with ^{89}Zr-cetuximab. RMPR at the time of the first scan (1 h) was 0.13 ± 0.03 (range, 0.09 - 0.16), whereas for the last scans (144 h) an increased RMPR of 0.49 ± 0.29 (range, 0.22 - 0.99) was observed. While varying the volumes employed in the bone marrow of the LV, we obtained bone marrow AC that deviated, at most 7%, when compared to AC_{RM} obtained from 30 mL bone marrow volumes. Typical coronal slices of ^{89}Zr-cetuximab images during the time course of 7 d can be seen in Figure 4.4.

The self RM dose estimate as calculated for the plasma based approach was 0.13 ± 0.05 mGy·MBq^{-1} (range, 0.08 - 0.24 mGy·MBq^{-1}, Figure 4.5).

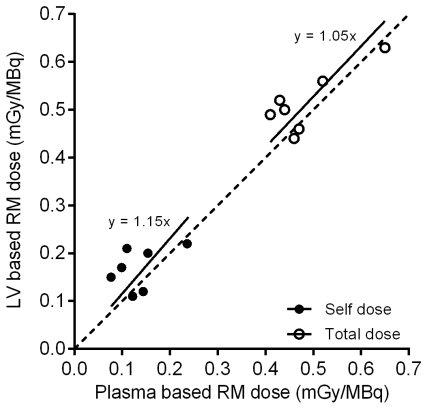

Figure 4.5. *RM dose estimates based on plasma and LV approach for self and total dose in ^{89}Zr-PET/CT studies. For radionuclides with little or no long range photon emission, such as ^{90}Y or ^{177}Lu, only the self dose component of the overall RM dose should be taken into account. Relative change in self RM dose between LV based and plasma based approaches was 21% (whereas in total RM dose this difference was diluted due to the cross dose contribution, and therefore, the average relative change in total dose was only 6%)*

Table 4.3. *RM absorbed dose*

Approach	Self dose mGy·MBq^{-1}	Cross dose mGy·MBq^{-1}	Total dose mGy·MBq^{-1}
Plasma	0.13 ± 0.05	0.35 ± 0.03	0.48 ± 0.08
LV	0.17 ± 0.04	0.34 ± 0.03	0.51 ± 0.06

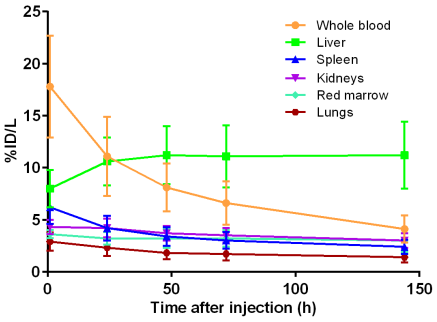

Figure 4.6. *Average %ID per litre as function of time after injection (with decay correction) for all visible organs. Error bars correspond to standard deviation as calculated for 7 patients.*

The LV based self RM dose estimate was 0.17 ± 0.04 mGy·MBq^{-1} (range, 0.11 - 0.22 mGy·MBq^{-1}). The total RM dose estimate for the plasma and LV based approaches was 0.48 ± 0.08 mGy·MBq^{-1} (range, 0.41 - 0.65 mGy·MBq^{-1}) and 0.51 ± 0.06 mGy·MBq^{-1} (range, 0.44 - 0.63 mGy·MBq^{-1}), respectively (Table 4.3). The contribution of cumulated activity before the first and after the last scan as compared with the total RM cumulated activity was 16% ± 2% and 27% ± 4% for plasma and LV based methods, respectively. In addition, across all patients, the self RM dose percentage contribution to the total RM dose varied from 18% to 35%, whereas the whole body to blood cumulated activity ratio varied from 3.4 to 1.8.

The organ average uptake for liver, lungs, kidneys, spleen, and RM is shown in Figure 4.6. The highest average absorbed dose was observed in the liver with 2.60 ± 0.78 0.06 mGy·MBq^{-1}, followed by the kidneys (1.04 ± 0.24 mGy·MBq^{-1}), spleen (0.89 ± 0.22 mGy·MBq^{-1}), lungs (0.66 ± 0.17 mGy·MBq^{-1}), and RM (0.51 ± 0.06 mGy·MBq^{-1}). The effective dose was calculated to be 0.61 ± 0.09 mSv·MBq^{-1}. All possible 3 time-point combinations were tested in estimating organ absorbed doses and effective doses. The 1h-48h-144h and the 48h-72h-144h protocols showed the smallest (<4%) and the largest (~20%) discrepancies, respectively, when compared with the 5 time-point dosimetry protocol (Table 4.4). Table 4.5 shows organ effective half-lives of ^{89}Zr-cetuximab for 1- to 72-h and 72- to 144-h time intervals. Whole body effective half-life was 70 ± 6 h for the whole imaging range.

Table 4.4. *Organ absorbed doses.* * *denotes that RM absorbed dose is based on manual delineation.*

mGy·MBq^{-1}	Kidneys	Liver	Liver excl. tumour	Lungs	Spleen	RM*	Remainder of the body	Effective dose mSv·MBq^{-1}
M-1	0.82	1.54	1.61	0.50	0.79	0.46	0.45	0.52
M-2	0.93	2.00	2.07	0.55	0.74	0.52	0.45	0.55
M-3	0.82	2.18	2.68	0.52	0.71	0.50	0.45	0.54
M-4	0.83	2.42	2.42	0.51	0.62	0.49	0.45	0.55
F-1	1.24	2.91	2.91	0.86	1.11	0.56	0.56	0.70
F-2	1.32	3.48	3.67	0.80	1.10	0.44	0.56	0.71
F-3	1.30	3.64	3.69	0.85	1.15	0.63	0.56	0.72
5 time-point dosimetry approach								
Mean	1.04	2.60	2.72	0.66	0.89	0.51	0.50	0.61
SD	0.24	0.78	0.78	0.17	0.22	0.06	0.06	0.09
Simplified 3 time-point dosimetry approach								
Mean	1.04	2.50	-	0.66	0.91	0.50	0.50	0.61
SD	0.22	0.75	-	0.17	0.22	0.06	0.06	0.09

Table 4.5. *Effective half-life (h)*

Organ	1-72 h after injection	72-144 h after injection
Kidneys	60 ± 10	63 ± 7
Liver	192 ± 61	79 ± 9
Lungs	41 ± 7	61 ± 9
Spleen	37 ± 8	57 ± 6
RM	71 ± 29	69 ± 14
Blood	30 ± 3	45 ± 3

4.4 Discussion

This study assessed PET/CT based biodistribution and dosimetry of ^{89}Zr-cetuximab for all organs with positive PET uptake. In addition, an image based approach for estimating the RM absorbed dose in ^{89}Zr PET/CT studies was compared with the conventional plasma based approach. While ^{18}F-FDG is a metabolic tracer that targets tumours in a nonspecific manner, radiolabelled mAbs target a specific tumour cell surface marker. That said, immunoPET can give insight on tumour targeting and on the amount of the mAb accumulated in the tumour, offering the opportunity to select those patients who will benefit from mAb-based therapy and allowing treatment planning to be tailored to the needs of each patient. More information on the potential added value of immunoPET in the clinical setting is presented by Wu (16).

The present study showed a nonconstant RMPR over time for ^{89}Zr-cetuximab. Hindorf et al. (6) have shown an increasing RMBLR for up to 6 d after the administration of ^{131}I-labelled anti-CD22 mAb in patients. Similar findings were reported by Schwartz et al. (5), who found an increasing RMPR with time after radiolabelled antibody administration for patients injected with ^{124}I-cG250 and ^{124}I-huA33. Perk et al. (1) demonstrated approximately 2.5 times higher accumulation of N-sucDf-^{89}Zr conjugates in bone over time 5.85 ± 1.05 percentage injected dose (%ID)·g^{-1} than for the RIT conjugates in tumour bearing nude mice studies at 72 h after injection. This is in agreement with a study by Chang et al. (17), who demonstrated an elevated bone uptake of 5.70 ± 3.00 %ID·g^{-1} at 120 h post-injection. In contrast, the present findings showed a constant RM uptake over time, which could be due to catabolism of cetuximab in the liver. Then the associated ^{89}Zr-containing metabolites re-enter the bloodstream and they redistribute in the bone marrow. Therefore, the increasing RMPR could be explained, at least in part, by the relative rapid washout of ^{89}Zr-cetuximab from the bloodstream in combination with the constant RM uptake. No foci of high activity were detected in bone sites.

The contribution of extrapolations in the cumulated activity before the first and after the last scan was below 20% as recommended by the dosimetry guidelines of European Association of Nuclear Medicine (18). In addition, the small interpatient variation of the extrapolations (data not shown) implies that the uncertainty due to extrapolations is comparable between patients. Although the whole body to blood cumulated activity ratio decreased, the self RM dose percentage contribution to the total RM dose increased, thus making any variations in parameters related to self RM dose, such as HCT and RMECFF, more important.

The estimation of self RM dose as determined with the LV based approach yielded, on average, 21% higher values than those obtained with the plasma based approach. This is due to the constant RMPR (0.19) used in the plasma based approach. The present findings suggest an increasing RMPR, thus making the latter approach inappropriate. In other words, the relative faster washout of ^{89}Zr-cetuximab from the plasma component, compared with the constant uptake in the RM, suggests that the plasma based approach may not provide for an accurate estimation of RM absorbed doses. The total RM doses based on plasma and LV approaches were within 6% of each other. However, for therapeutic analogues with no or little emissions of long range photons (depending on their energy and half-life) only the self RM dose term is relevant.

The absorbed dose estimates in the present study are in line (within

20% for all organs except liver) with previous ^{89}Zr-labelled studies. Rizvi et al. (2) reported that, for ^{89}Zr-ibritumomab tiuxetan, the liver was the organ with the highest absorbed dose (1.36 ± 0.58 mGy·MBq^{-1}), followed by the spleen (1.04 ± 0.16 mGy·MBq^{-1}), kidneys (0.75 ± 0.06 mGy·MBq^{-1}), lungs (0.63 ± 0.11 mGy·MBq^{-1}), and RM (0.46 ± 0.05 mGy·MBq^{-1}), whereas the effective dose was found to be 0.55 ± 0.07 mSv·MBq^{-1}. Borjesson et al. (19) in a radiation dosimetry study of ^{89}Zr-cmAb U36 found the highest absorbed dose for the liver (1.30 ± 0.34 mSv·MBq^{-1}), followed by the kidneys (1.00 ± 0.30 mSv·MBq^{-1}), lungs (0.79 ± 0.26 mSv·MBq^{-1}), and spleen (0.72 ± 0.18 mSv·MBq^{-1}). The effective dose was estimated to be 0.60 ± 0.04 mSv·MBq^{-1}. However, a direct comparison of organ absorbed dose estimates between ^{89}Zr-labelled cetuximab and other ^{89}Zr-labelled mAbs should be interpreted with care, because metabolism in the liver and specific targeting of each mAb may vary. ^{89}Zr-cetuximab is used only for diagnostic purposes, and therefore the effective dose was presented. But in the setting of radioimmunotherapy the dose on a tumour or the RM should be presented as absorbed dose as well. Because no tumour data are discussed in this article, only RM absorbed dose data have been reported. With regards to effective half-lives, only 1 immunoPET study reports on ^{89}Zr effective half-lives and more specifically in whole body biological clearance (20). This was found to be 219 h on average, and it can be translated to 58 h on the whole body effective half-life. This figure is somewhat comparable to the 70 h seen in the current study. We split the image data points into 2 time intervals in order to gain insight of organ kinetics over time. With regards to the simplified 3 time-point dosimetry protocol, the first time-point (1 h) is of importance, because the use of it will lead to more accurate absorbed dose estimations than when using the 24 h scan. In addition, ^{89}Zr labelled mAbs exhibit slow kinetics; thus, targeting of specific organs or tumours will occur in late time-points, making the 144 h time-point essential in a simplified protocol. The present study suggests that a simplified 3 time-point dosimetry approach may be used for organ absorbed dose estimation as an alternative to the reference approach, because it yielded similar results (within ~4%). This will reduce the total scanning time, avoiding unnecessary discomfort and additional radiation burden (due to additional low-dose CT scans) to the patient and without compromising accuracy in dose estimation.

There are technical factors that may hamper accurate quantification of RM activity concentration and thus absorbed dose estimation. From a technical point of view, partial-volume effect might have resulted in underestimation of RM activity concentrations. On the basis of ^{89}Zr phantom studies (21), the activity concentration of a 2.5 cm sphere surrounded by

a homogeneous background can be underestimated by as much as 20%. Nevertheless, the present observation of a nonconstant (increasing) BM-to-background ratio as function of time indicates that partial volume corrections based on a fixed factor taken from phantom studies (with sphere-to-background ratio of 10) would provide misleading results. Schwartz et al. (5) used recovery coefficients for partial volume correction derived from phantom studies. Unfortunately, there was no report on how the BM-to-background ratio behaved over time, because a nonconstant ratio would require a time-varying partial volume correction. Notably, the current study showed small deviations in AC_{RM} while varying the VOIs, indicating a minimal impact of the partial-volume effect. In addition, the 6 mL VOIs were employed on the LV segments such that a distance of at least 1 cm (2 scanner spatial resolution) from the outer LV bone was ensured. In any case, even if partial-volume corrections were applied, it would only increase the dissociation of RM dose estimation between image and plasma based approaches.

4.5 Conclusion

Total RM dose estimates derived from plasma and image based approaches are equal within 6%. For dosimetry purposes in immunoPET this would be acceptable. Nevertheless, an image based approach, using manual delineation of the LV, is preferred for determining RM dose estimates, because it accounts for a non-constant RMPR. The liver showed the highest absorbed dose amongst all organs, and the effective dose was 0.61 ± 0.09 mSv·MBq^{-1}. A simplified approach using 3 time points appears to be feasible, reducing logistical costs and scanning time required.

Appendix

Plasma based RM dosimetry. The total RM dose consistes of a self dose (patient mass-independent) and a cross dose (patient mass-dependent) term:

$$D_{RM}^{Total} = \tilde{A}_{RM} \times S\left(RM \leftarrow RM\right) + \left(\tilde{A}_{WB} - \tilde{A}_{RM}\right) \times S\left(RM \leftarrow RB\right) \quad (4.7)$$

The dose conversion (S) factors for both RM and remainder-of-body contribution should be mass adjusted, as follows:

$$S\left(RM \leftarrow RM\right) = S\left(RM \leftarrow RM\right)_{MIRD3} \times \frac{m_{RM-MIRD3}}{m_{RB-patient}} \quad (4.8)$$

$$S(RM \leftarrow RB) = \left\{ S(RM \leftarrow WB)_{MIRD3} \times \frac{m_{WB-MIRD3}}{m_{RB-MIRD3}} - S(RM \leftarrow RM)_{MIRD3} \times \frac{m_{RM-MIRD3}}{m_{RB-MIRD3}} \right\} \times \times \frac{m_{RM-MIRD3}}{m_{RB-patient}} \quad (4.9)$$

Final expressions for both self dose and cross dose to RM are obtained by substituting equations 4.2, 4.8 and 4.9 into 4.7:

$$D_{RM}^{Self} = RMECFF \times \left[\tilde{A}_{PL}\right] \times m_{RM-MIRD3} \times S(RM \leftarrow RM)_{MIRD3} \quad (4.10)$$

$$D_{RM}^{Cross} = \left\{ \tilde{A}_{WB} - \left[\tilde{A}_{PL}\right] \times RMECFF \times \frac{m_{RM-MIRD3}}{m_{WB-MIRD3}} \times m_{WB-patient} \right\} \times \times \left\{ S(RM \leftarrow WB)_{MIRD3} \times \frac{m_{WB-patient}}{m_{WB-patient} - m_{RM-patient}} - S(RM \leftarrow RM)_{MIRD3} \times \frac{m_{RM-patient}}{m_{WB-patient} - m_{RM-patient}} \right\} \times \times \frac{m_{WB-MIRD3}}{m_{WB-patient}} \quad (4.11)$$

Image based RM dosimetry. Here, the average activity concentration in the red marrow is used for self and cross RM dose estimation. Equations 4.10 and 4.11 can be rewritten as follows:

$$D_{RM}^{Self} = \left[\tilde{A}_{RM}\right] \times m_{RM-MIRD3} \times S(RM \leftarrow RM)_{MIRD3} \quad (4.12)$$

$$D_{RM}^{Cross} = \left\{ \tilde{A}_{WB} - \left[\tilde{A}_{RM}\right] \times \frac{m_{RM-MIRD3}}{m_{WB-MIRD3}} \times m_{WB-patient} \right\} \times \times \left\{ S(RM \leftarrow WB)_{MIRD3} \times \frac{m_{WB-patient}}{m_{WB-patient} - m_{RM-patient}} - S(RM \leftarrow RM)_{MIRD3} \times \frac{m_{RM-patient}}{m_{WB-patient} - m_{RM-patient}} \right\} \times \times \frac{m_{WB-MIRD3}}{m_{WB-patient}} \quad (4.13)$$

References

[1] L.R. Perk, G.W. Visser, M.J. Vosjan, M. Stigter van Walsum, B.M Tijink, and C.R. Leemans G.A. van Dongen. (89)zr as a pet surrogate radioisotope for scouting biodistribution of the therapeutic radiometals (90)y and (177)lu in tumor-bearing nude mice after coupling to the internalizing antibody cetuximab. *J Nucl Med*, 46: 1898–1906, 2005.

[2] S.N. Rizvi, O.J. Visser, M.J. Vosjan, A. van Lingen, O.S. Hoekstra, J.M. Zijlstra, P.C. Huijgens, G.A. van Dongen, and M. Lubberink. Biodistribution, radiation dosimetry and scouting of 90y-ibritumomab tiuxetan therapy in patients with relapsed b-cell non-hodgkin's lymphoma using 89zr-ibritumomab tiuxetan and pet. *Eur J Nucl Med Mol Imaging*, 39:512–520, 2012.

[3] L. Koi, R. Bergmann, K. Bruchner, J. Pietzsch, H.J. Pietzsch, M. Krause, J. Steinbach, D. Zips, and M. Baumann. Radiolabeled anti-egfr-antibody improves local tumor control after external beam radiotherapy and offers theragnostic potential. *Radiother Oncol*, 110:362–369, 2014.

[4] G. Sgouros. Bone marrow dosimetry for radioimmunotherapy: theoretical considerations. *J Nucl Med*, 34:689–694, 1993.

[5] J. Schwartz, J.L. Humm, C.R. Divgi, S.M. Larson, and J.A. O'Donoghue. Bone marrow dosimetry using 124i-pet. *J Nucl Med*, 53:615–621, 2012.

[6] C. Hindorf, O. Linden, J. Tennvall, K. Wingardh, and S.E. Strand. Time dependence of the activity concentration ratio of red marrow to blood and implications for red marrow dosimetry. *Cancer*, 94(4 Suppl):1235–1239, 2002.

[7] Y. Zhou, K.E. Baidoo, and M.W. Brechbiel. Mapping biological behaviors by application of longer-lived positron emitting radionuclides. *Adv Drug Deliv Rev*, 65: 1098–1111, 2013.

[8] W.B. Nagengast, E.G. de Vries, G.A. Hospers, N.H. Mulder, J.R. de Jong, H. Hollema, A.H. Brouwers, G.A. van Dongen, L.R. Perk, and M.N. Lub de Hooge. In vivo vegf imaging with radiolabeled bevacizumab in a human ovarian tumor xenograft. *J Nucl Med*, 48:1313–1319, 2007.

[9] T.H. Oude Munnink, M.E. Arjaans, H. Timmer-Bosscha, C.P. Schrder, J.W. Hesselink, S.R. Vedelaar, A.M. Walenkamp, M. Reiss, R.C. Gregory, M.N. Lub de Hooge, and E.G. de Vries. Pet with the 89zr-labeled transforming growth factor-beta antibody fresolimumab in tumor models. *J Nucl Med*, 52:2001–2008, 2011.

[10] S. Surti, A. Kuhn, M.E. Werner, A.E. Perkins, J. Kolthammer, and J.S. Karp. Performance of philips gemini tf pet/ct scanner with special consideration for its time-of-flight imaging capabilities. *J Nucl Med*, 48:471–480, 2007.

[11] M.G. Stabin, R.B. Sparks, and E. Crowe. Olinda/exm: the second-generation personal computer software for internal dose assessment in nuclear medicine. *J Nucl Med*, 46:1023–1027, 2005.

[12] H.N. Greuter, R. Boellaard, A. van Lingen, E.J. Franssen, and A.A. Lammertsma. Measurement of 18f-fdg concentrations in blood samples: comparison of direct calibration and standard solution methods. *J Nucl Med Technol*, 31:206–209, 2003.

[13] S. Shen, G.L. Denardo, G. Sgouros, R.T. O'Donnell, and S.J. DeNardo. Practical determination of patient-specific marrow dose using radioactivity concentration in blood and body. *J Nucl Med*, 40:2102–2106, 1999.

[14] M.G. Stabin, J.A. Siegel, and R.B. Sparks. Sensitivity of model-based calculations of red marrow dosimetry to changes in patient-specific parameters. *Cancer Biother Radiopharm*, 17:535–543, 2002.

[15] A.H. Beddoe, P.J. Darley, and F.W. Spiers. Measurements of trabecular bone structure in man. *Phys Med Biol*, 21:589–607, 1976.

[16] A.M. Wu. Antibodies and antimatter: the resurgence of immuno-pet. *J Nucl Med*, 50:2–5, 2009.

[17] A.J. Chang, R.A. De Silva, and S.E. Lapi. Development and characterization of 89zr-labeled panitumumab for immuno-positron emission tomographic imaging of the epidermal growth factor receptor. *Mol Imaging*, 12:17–27, 2013.

[18] C. Hindorf, G. Glatting, C. Chiesa, O. Lindn, and G. Flux. Eanm dosimetry committee guidelines for bone marrowand whole-body dosimetry. *Eur J Nucl Med Mol Imaging*, 37:1238–1250, 2010.

[19] P.K. Borjesson, Y.W. Jauw, R. de Bree, J.C. Roos, J.A. Castelijns, C.R. Leemans, G.A. van Dongen, and R. Boellaard. Radiation dosimetry of 89zr-labeled chimeric monoclonal antibody u36 as used for immuno-pet in head and neck cancer patients. *J Nucl Med*, 50:1828–1836, 2009.

[20] N. Pandit-Taskar, J.A. O'Donoghue, and V. Beylergil et al. 89zr-huj591 immuno-pet imaging in patients with advanced metastatic prostate cancer. *Eur J Nucl Med Mol Imaging*, 41:2093–2105, 2014.

[21] N.E. Makris, R. Boellaard, E.P. Visser, J.R. de Jong, B. Vanderlinden, R. Wierts, B.J. van der Veen, H.J. Greuter, D.J. Vugts, G.A. van Dongen, A.A. Lammertsma, and M.C. Huisman. Multicenter harmonization of 89zr pet/ct performance. *J Nucl Med*, 55:264–267, 2014.